Nanotechnology Perceptions
ISSN 1660-6795
www.nano-ntp.com

Green synthesis of Gold Nanoparticles by using Nymphaea stellata: in-vitro Evaluation against Hepatic Cancer Cells

Rohit Tripathi[1,2], Arpita Yadav[3], Sudheer Kumar[4], Bhupendra Singh[5,6], Vikas Kumar[7,8], Amita Verma[1*]

[1]Bioorganic and Medicinal Chemistry Research Laboratory, Department of Pharmaceutical Sciences, Sam Higginbottom University of Agriculture, Technology & Sciences, Prayagraj, 211007, India
[2]Department of Pharmaceutical chemistry,Shambhunath Institute of Pharmacy, Prayagraj,211012, India
[3]Bhagwati college of Pharmacy,Baraut,Baghpat, 250611,India
[4]Department of Biotechnology, National Institute of Pharmaceutical Education and Research Hajipur, Bihar, 844102, India
[5]School of Pharmacy, Graphic Era Hill University, Dehradun, Uttrakhand, 248002, India
[6]Department of Pharmacy,S.N.Medical College, Agra, 282002, India
[7]Natural Product Research Laboratory, Department of Pharmaceutical Sciences, SamHigginbottom University of Agriculture, Technology & Sciences, Prayagraj, 211007, India
[8]University Centre for Research and Development, Chandigarh University, Gharuan 140413, Punjab, India
Email: amitaverma.dr@gmail.com

Objective: This study was designed to evaluate the green synthesis of gold nanoparticles: characterization and evaluation of anticancer activity using Nymphaea stellata aerial parts extract against liver cancer cell line (HepG2). Materials and Methods: Gold nanoparticles were synthesized from N. stellata aerial parts extract and characterized by using different techniques such as UV, FTIR, Zeta potential, DLS, SEM, and TEM. The in-vitro anticancer activity against the liver cancer cell line HepG2 was evaluated by MTT assay. Total phenolic content (TPC) and total flavonoids content (TFC) of plant extract and antioxidant activity by DPPH and FRAP were also done. Results: The phytoconstituents present in arial parts plant extract such as steroids, alkaloids,

phenols, flavonoids, saponins, tannins and anthraquinones were identified in N. stellata. Gold nanoparticles were characterized by using the techniques of UV, FTIR, Zeta potential, DLS, SEM, and TEM. The developed nanoparticles effectively inhibited HepG2 cell growth by MTT assay. TPC and TFC for plant extract was found to be 48.16 mg/gm and 42.33mg/gm. FRAP assay for extract and NS-GNP showed 40.87µg/ml and 64µg/ml. In DPPH assay, IC50 for extract and NS-GNP was found to be 90.4µg/ml and 75.75µg/ml. The developed NS-GNP effectively inhibited HepG2 cell growth by MTT assay with IC50 value 95.74 µg/ml. Conclusion: It can be concluded that synthesized gold nanoparticles by using green approach showed significant anticancer potential against Hep G2 cell line.

Keywords: Green synthesis, gold nanoparticles, N. stellata, liver cancer cells, HepG2 cells.

1. Introduction

Primary liver cancer ranks as the fifth most frequently diagnosed malignancy and the third foremost cause of mortality worldwide. Hepatocellular carcinoma (HCC) constitutes over 85% of all primary liver malignancies. Cancer is among most fatal disease with leading cause of death worldwide that affects individuals who face physical suffering, diagnostic procedures, mental stress, chemo-therapies, after-effects of treatment, with poor and reduced life expectancy. Primary liver cancer is the sixth most frequent cancer and second chief cause of cancer mortality across the globe. It is a major challenge for public health, its diagnosis and treatment planning is very important for its control. Its prevention and control programmes as vaccination at birth, particularly in endemic countries like China, have significantly reduced the incidence of primary liver cancer and burden of liver disease is planned to be further reduced globally by 2030 according to World Health Organization (WHO) (Losic et al., 2020). An estimated 564,000 new cases are recorded each year, with 166,000 women and 398,000 men affected. Liver cancer can develop before the age of 20 in high-risk countries, although it is rare in low-risk countries before the age of 50. The considerable disparities in morbidity and mortality rates reflect the unequal distribution of primary risk factors. Chronic hepatitis B virus infection is a major risk factor for liver cancer in most areas where it is prevalent.

Hepatitis B virus (HBV) infection with ingestion of food infected with aflatoxin B1, a mycotoxin. Conversely, in the majority of low-incidence regions, the principal risk factors are hepatitis C virus (HCV) infection, excessive alcohol intake, obesity, and diabetes. Liver fibrosis is sometimes associated with hepatocellular carcinoma (HCC), and in its extreme stages, it may lead to significant cirrhosis. The history of liver disease influences the prognosis of liver cancer (Thorgeirsson et al., 2002).This is because hepatocytes sustain damage from oxidative stress and reactive oxygen species build up in the organ during fibrotic condition As a result, there is a need for safe, affordable, and efficient solutions to treat the illness (Ghany et al., 2003).Selected Nymphaea stellata Willd plant for this work belonging to family Nymphaeaceae, well known medicinal plants. Besides being the ornamental plant, many parts of this plant have been demonstrated to possess several

medicinal values. It is a member of Lotus family, an evergreen large, perennial aquatic herb with a short, ovoid and acute root stock. Various solvent extract of the complete plant have demonstrated the presence of sterols, alkaloids, saponins, tannins, flavonoids, and phenolic compounds. The primary phytochemical of the plant Nymphayol has been utilized in Ayurveda for the treatment of liver diseases since ancient times (Antonisamy et al., 2014).

2. Role of flavonoids in liver cancer

The phytoconstituents present in the selected plant Nymphaea stellata such as flavonoids like Campesterol, Stigmasterol, Nymphyol etc are helpful in destroying liver cancer cells. Chemo prevention approaches based on phytochemicals found in food are becoming increasingly essential in the treatment and cure of cancer (Raja et al., 2010). We have highlighted the most important flavonoid phytoconstituents utilized as anti-cancer medications to treat and prevent liver cancer. Flavonoids' potential to influence several signal transduction pathways within neoplastic cells is linked to their anti-cancer properties. Flavonoids can promote cellular differentiation and angiogenesis, limit cancer cell proliferation and spread, arrest the cell cycle, and induce apoptosis in malignant cells (Baby et al., 2021). Flavonoids in the diet may also help to improve the efficacy of cancer treatments and reduce the risk of acquiring cancer. Numerous in-vitro and in-vivo studies have demonstrated that flavonoids can overcome medication resistance while under therapy. Numerous epidemiologic studies have indicated that particular flavonoids, diets, or foods high in flavonoids can help prevent tumors, slow tumor growth, and lower the level of established high-risk indicators. However, current evidence suggests that adding flavonoids to established anti-cancer therapies may be beneficial, while further research is needed. The field of nano-based delivery has grown significantly to transport native forms of key chemicals and therapeutic agents for the treatment of a variety of diseases. A wide range of nanomaterials are used in the drug delivery procedure to carry the treatment to the designated target site (Biharee et al., 2023; K. Singh et al., 2022). (Fig.1) presents the role of flavonoids in the treatment of liver cancer.

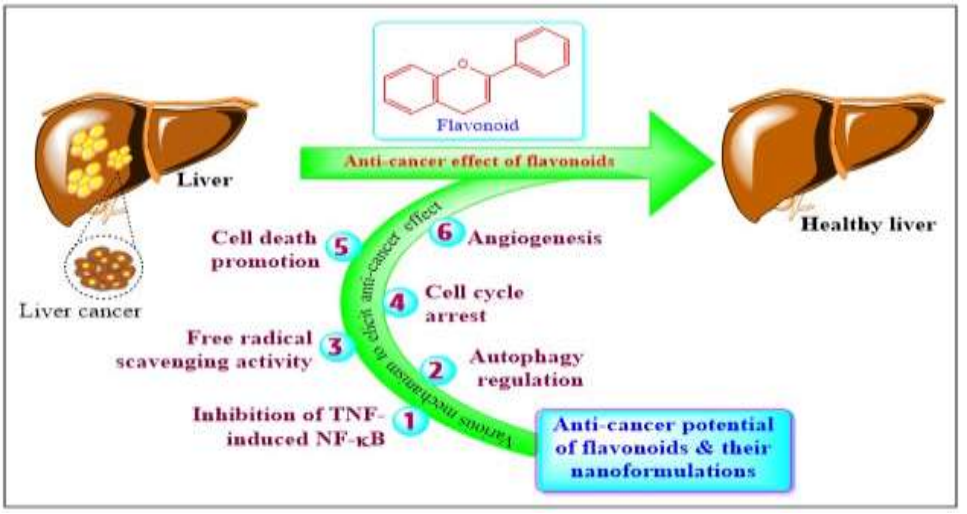

Figure1: Role of flavonoids in liver cancer exploration of their Cytotoxic Effects

3. Material and Methods

3.1. Collection, authentication and extraction of plant material: Plant was collected from the CSIR-CIMAP, Lucknow India, and authenticated by the Botanical Survey of India, Allahabad with reference no. SIP/2021/168. The collected plant material was air dried and powdered. Plant extract was prepared by boiling 10 gm of powder with 100 ml of deionized water for 10 minutes and filtered through Whatman filter paper. Some used chemicals as Auric chloride ($HAuCl_3$), sodium hydroxide (NaOH, 99%), solvents as ethanol (C_2H_5OH, 99%), ethyl acetate ($C_4H_8O_2$, 99%), n-Hexane (C_6H_{14}, 99%) purchased from Sigma-Aldrich.

3.2. Phytochemical investigation: Phytochemical analysis of the extract was carried out to confirm the presence of carbohydrates, proteins, flavonoids, and polyphenols. The standard Molisch test was utilized for detecting carbohydrates, while the Ninhydrin test was employed for protein detection. The Shinoda test successfully identified flavonoids (Czeczot et al.,1990). Dragendorff's test confirmed the presence of alkaloids. Foam test validated the existence of Saponins, Bontrager's Test was detecting glycosides, and the silver mirror test provided conclusive evidence of the presence of phenolic components and alkaline reagent test confirm the presence of flavonoids. (Loncaricet al.,2020).

3.3. Total flavonoid content (TFC): TFC was performed using the aluminium chloride method. 0.5 mL of aqueous plant extract (NS) was mixed with 1 mL of 2% $AlCl_3$ generated in methanol solution and incubated for 10-12 minutes at room temperature. The absorbance was measured at 430 nm. The measurements were taken using the flavonoids quercetin (QE) as the standard, with units of µg/ml, QE/g dry extract (Kalita et al., 2013).

3.4. Total phenolic content (TFC):0.2 ml of Folin-Ciocalteu reagent (FCR) 10% v/v was added to 0.1 ml of sample solution. The mixture was pooled for 5 minutes before adding 0.8 ml of $CaCO_3$ 7.5% w/v and incubating for 2 hours at 25˚C. The absorbance was measured at 765 nm. Calibration curve of a standard gallic acid solution represented as mg gallic acid equivalents (GAE) per gram of extract (Babbar et al., 2011).

3.5. Diphenylpicryl hydrazine (DPPH): The capacity of the different materials to donate hydrogen or scavenge radicals was evaluated using the stable DPPH radical, 0.75 mL of sample solution at different concentrations ranging from 1 to 500 µg mL^{-1} was mixed with 1.5 mL of a DPPH methanolic solution (20 mg L^{-1}). After 20 minutes of processing, 517 nm was the wavelength to measure absorbance. And calculate the percentage inhibition by using the given formula.

$$\% \text{ Inhibition } = \left(\frac{\text{A control} - \text{A sample}}{\text{A control}}\right) \text{X100}$$

Where $A_{control}$ and A_{sample} are the absorbance value of control and sample

The decoloration was graphed versus the sample concentration, a regression curve was constructed, and the IC50 value was determined. IC50 refers to the quantity of sample required to reduce the absorbance of DPPH by 50%. The results are presented as antiradical efficiency (AE), defined as the reciprocal of the IC50 value multiplied by 1000 (AE = 1000/IC50) (Saravanan et al., 2010).

3.6. FRAP assay: The ferric tripyridyltriazine [Fe(III)-TPTZ] complex requires reduction by

a reductant at low pH to yield ferrous TPTZ (Fe(II)-TPTZ). Ascorbic acid (10 mg/10 ml) used as the reference for the linear calibration curve. The stock solution was formulated as follows: 300 mM acetate buffer solution comprising (3.1 grams of sodium acetate trihydrate and 16 ml of acetic acid) pH 3.6; 10 mM TPTZ (2, 4, 6-tripyridyl-striazine) solution in 40 mM HCl; and a 20 mM iron (III) chloride hexahydrate solution. A workable solution was prepared by combining 25 ml of acetate buffer, 2.5 ml of TPTZ solution, and 2.5 ml of iron (III) chloride hexahydrate solution. The final temperature was sustained at 37°C prior to start the work. The sample (150 µL, equivalent to 0.15 mL) was react with 2850 µL (2.85 mL) of the FRAP solution for 30 minutes in a dark environment. The measurement was performed at 593 nm, indicating the amount required to reduce the Fe^{+3}-Fe^{+2} ratios when measuring absorbance at 593 nm (Guo et al., 2003).

3.7. Synthesis of gold nanoparticles: A measured amount of gold chloride (17 mg) was placed in a 100 mL volumetric flask and to prepare a 0.5mM gold chloride solution, the volume was adjusted to the mark using deionized water. Gold nanoparticles (GNP) were synthesized by combining aqueous plant extracts (NS) with aqueous gold chloride solutions (0.5 mM) at room temperature. The development of GNP was indicated by a visible color change. The bioreduction of gold salt was examined by evaluating 0.1 ml aliquots of the mixture at regular intervals using UV-Visible spectroscopy following appropriate dilutions. The mixture was centrifuged by utilizing a refrigerated high-speed centrifuge at 17,000 rpm for 20 minutes. GNP pellets were isolated, and re-suspended in fresh deionized water, followed by centrifugation three times to eliminate the excess phytochemicals (Mahakham et al., 2016).

3.8. Characterization of synthesized nanoparticles: Synthesized nanoparticles were evaluated using ultraviolet (UV) spectrophotometry, Fourier transform infrared spectroscopy (FT-IR), dynamic light scattering (DLS), transmission electron microscopy (TEM), scanning electron microscopy (SEM), and Zetasizer analyses. UV spectroscopic analyses revealed a distinct UV-Visible peak, indicating the synthesis of NS-GNP. FT-IR, XRD, and DLS were employed to ascertain the surface properties (presence of phytoconstituents) and crystalline structure of LE-GNP, respectively. The TEM, SEM, and Zetasizer analyses indicated a particle size.

3.9. In Vitro Cytotoxicity Evaluation: The cytotoxicity of the provided samples on the HepG2 cell line (obtained from NCCS Pune) was evaluated using the MTT test. Ten thousand cells per well were grown in a 96-well plate for 24 hours in DMEM (Dulbecco's Modified Eagle Medium-AT149-1L) supplemented with 10% FBS (Fetal Bovine Serum - HIMEDIA-RM 10432) and 1% antibiotic solution at 37°C with 5% CO_2. The subsequent day, the cells were subjected to different concentrations. Untreated cells were classified as the control group. After 24 hour incubation, MTT Solution was added to the cell culture and incubated for an additional 2 hours. Following the experiment, the culture supernatant was discarded, and the cell layer matrix was solubilized in 100 µl of Dimethyl Sulfoxide, subsequently examined using an ELISA plate reader (iMark, Biorad, USA) at wavelengths of 540 nm and 660 nm. IC50 was ascertained using Graph Pad Prism-6 program (Grela et al., 2018).

4. Result and Discussion:

4.1. Characterization of NS-GNP:

4.1.1. UV-Vis spectroscopy:The UV-Vis spectrum of plant extract and their synthesized NS-GNP is illustrated in (Fig. 2a), UV-Vis absorption spectra exhibited a pronounced and extensive peak for plant extract rich in flavonoids is typically at 230-380 (nm) and for synthesized NS-GNP absorption at 530 nm due to surface plasmon resonance (SPR) in (Fig. 2b). The significant absorption of electromagnetic waves in the visible spectrum is attributed to metal nanoparticles, where surface plasmon resonance (SPR) occurs due to the collective oscillations of conduction electrons when irradiated by visible light. The color shift of NS-GNP in aqueous solution, attributed to stimulation in the UV-visible band, indicates that NS-GNP synthesis. (Zimbone et al., 2011).

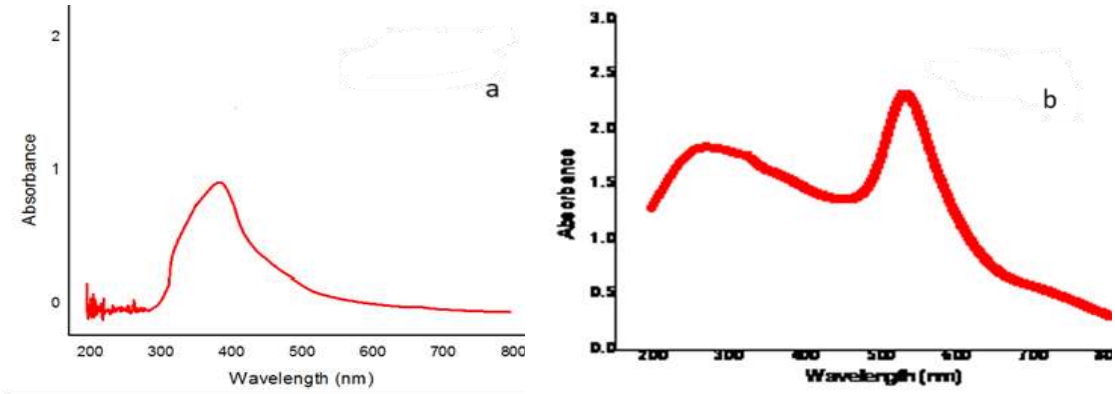

Figure 2: a) UV-Vis spectroscopy of NS plant extract, b) synthesized NS-GNP

4.1.2. Fourier-transform infrared spectroscopy (FTIR): The fourier transform infrared spectroscopy spectra of N. stellata plant extract and their GNP were recorded by FTIR Spectrometer. The large peak seen around 3200-3500 cm^{-1} typically corresponds to O-H stretching vibrations, indicating the possibility of hydroxyl groups from the extract molecules adsorbed onto the GNP surface, which may add to the nanoparticles' stability. Peaks in the 1600-1750 cm^{-1} range may indicate carbonyl (C=O) stretching vibration. Depending on the biomolecules present in the extract, these peaks could represent amides (proteins), ketones, or carboxylic acids. Their presence suggests the attachment of these functional groups from the extract to the GNP surface. The fingerprint region (below 1500 cm^{-1}) often exhibits complexity and reflects the specific biomolecules present in the extract. Depending on the plant material, various peaks corresponding to functional groups such as C-N stretches (amines), C-O stretches (ethers), or aromatic rings may be discerned (Fig.3a) (Petiboiset al., 2001).

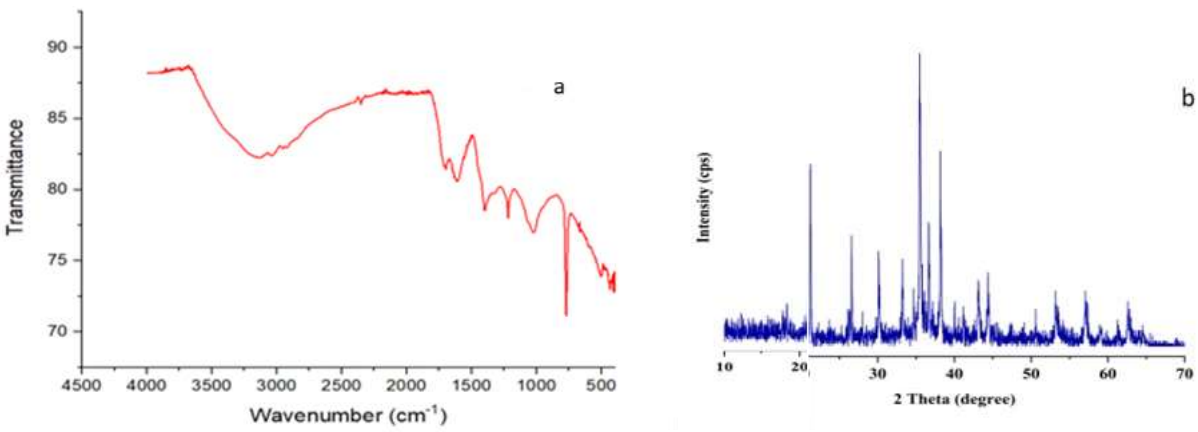

Figure 3: a) FTIR spectrum, b) XRD spectrum of synthesized NS-GNP

4.1.3. XRD pattern for crystalline nature of NS-GNP: In the X-ray diffraction pattern of N. stellata plant extract ($n\lambda = 2d\sin\theta$) attributed to the presence of crystalline carbon (d= 0.4305 nm, d>0.34) (Fig.3b) Schmidt and W., (2009).

4.1.4. Size distribution and surface charge characterization (zeta potential): The Zetasizer (Malvern Instruments, UK) was utilized to examine the particle size, particle size distribution, polydispersity index (PDI), and zeta potential of GNP. The mean droplet size and zetapotential of selected N. Stellata were found. The selected NS-GNP showed a negative zeta potential value with a non-significant difference among them. Nanoparticles with high zeta potential values are electrically more stable and can resist aggregation. The NS-GNP in the solution was uniform in size, partially aggregated, and stable. Zeta potential refers to the electrokinetic potential in colloidal systems. When positive and negative charges are present, more negative charges increase repulsive interactions, leading to more stable particles and preventing aggregation. To determine the zeta potential, 1ml of the diluted nanoparticle suspension was vortexes for 5 minutes, and then the zeta potential value was measured. The obtained value of -13.22 mV indicates that the nanoparticles are neutral in nature, ensuring stability in the chosen dispersant (Fig. 4a) Bhattacharjee and S., (2016).

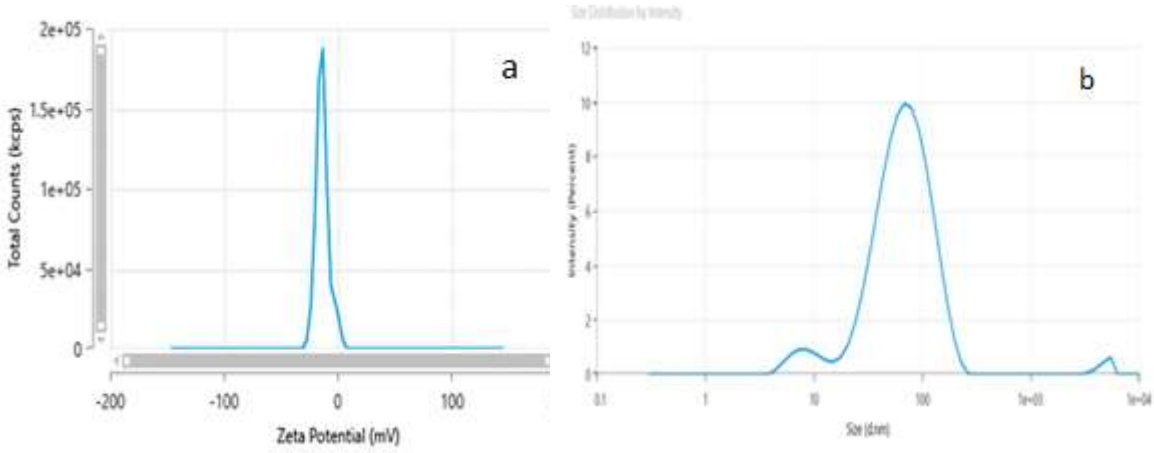

Figure 4: a) Zeta potential, b) DLS spectrum of synthesized NS-GNP

4.1.5. Dynamic Light Scattering (DLS) Measurement of NS-GNP: Dynamic light scattering (DLS) measurement was used to ensure the particle size of gold nanocomposite in an aqueous solution. It is the most reliable technique for evaluating any nano-material's particle size and size distribution in a solution. The size, surface charge, and colloidal stability of nanoparticles are assessed through this technique and expressed as Z-average. DLS analysis ensures that no aggregates are formed. This technology was employed after diluting formulations 100-fold with distilled water. Nanoparticles are tailored to target cells and specific physicochemical properties. The DLS measurements revealed that nanoparticles with a more negative charge had slightly smaller diameters, suggesting an influence of charge on behavior. The study indicated an average particle diameter of 53.18 nm and a polydispersity index of 0.319 (Fig.4b). A smaller diameter signifies a uniform distribution of particles within the formulation, unaffected by hydrodynamic diameter (Jans et al., 2009).

4.1.6. Scanning electron microscope (SEM): Data comprises SE-Imaging utilizing the ETD detector at appropriate accelerating voltage and current. The SEM (EVO 18 from Carl Zeiss, Germany) Quanta 200, outfitted with an EDAX system, was utilized to evaluate GNP. The sample was placed on a carbon grid and dried under low vacuum conditions (10-130 pa) at a voltage of 20 kV. The image was initially scanned at 3000x magnification, during which a specific region was examined using EDAX to confirm the presence of gold metal. Upon confirmation, photos were then scanned at magnifications of 6000x and 12000x and documented. (Fig. 5a) and (Fig. 5b) showed the particle size and presence of Au in GNP (Kubiak et al., 2016).

4.1.7. Transmission Electron Microscopy (TEM): TEM examination revealed the dimensions and morphology of the N. stellata gold nanoparticles. The TEM images indicate that gold nanoparticles are spherical, polydisperse, and exhibit a range of sizes. The Transmission Electron Microscope (TEM), Model FEI Themis 60-300, equipped with an EDS detector and FEI-Ceta 4kX4 camera, at the Indian Institute of Technology Gandhinagar (India), was utilized to examine the morphology and structural characteristics of the gold nanoparticles. Prior to analysis, the samples were deposited onto grids stained with 2% w/v

phosphotungstic acid for 30 seconds following a dilution of 20–100 times with deionized water. The grids were subsequently dried and analysed by a combination of bright field imaging at different magnifications to elucidate the shape and size of the droplets.(Fig. 5c)(Goldstein et al.,2014)

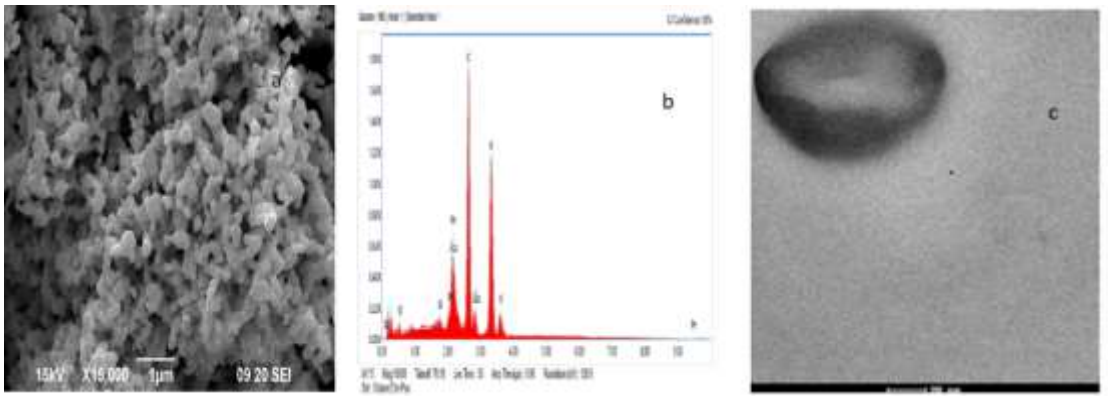

Figure 5: a) SEM image, b) SEM-EDAX, c) TEM of GNP

4.2. Estimation of total phenolic content (TPC) and total flavonoids content (TFC):

The UV-vis, colorimetric method was used to determine total phenolic and total flavonoid content in Plant extract. Total phenolic content was found to be 48.16 mg of gallic acid equivalents (GAE)/g of dry extract standard calibration graph is shown in (Fig. 6a). Flavonoid content was observed to be 42.33 mg of quercetin equivalents (QE)/g of dry extract for this standard calibration graph is shown in (Fig. 6b).

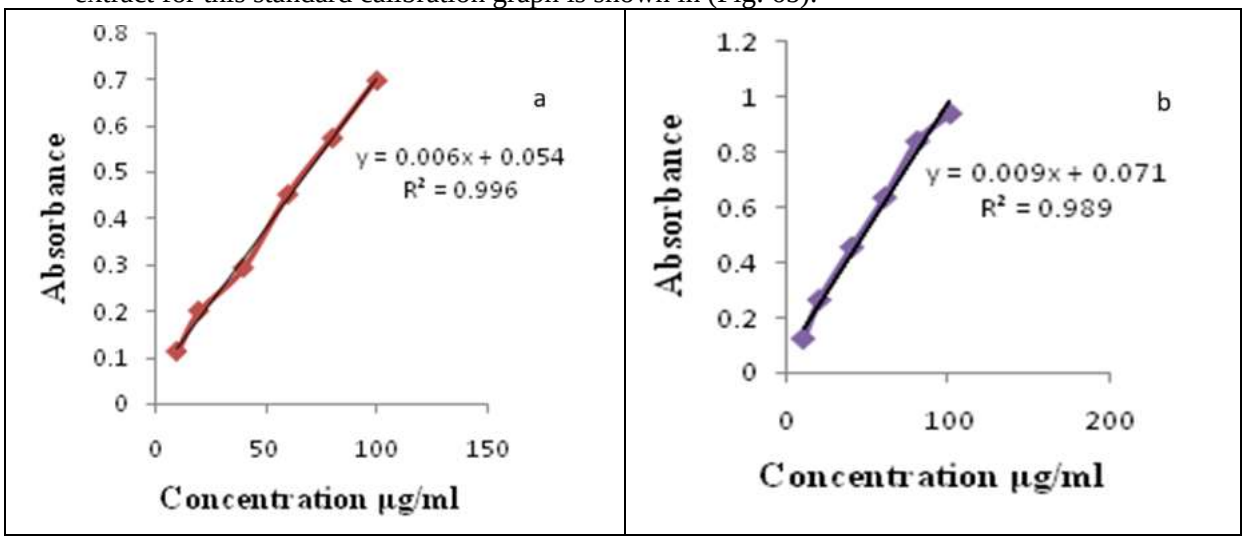

Figure 6: a) Standard calibration graph of Gallic acid (GA), b) Quercetin (QE)

4.3. Antioxidant assay FRAP and DPPH

FRAP assay of the plant extract (NS) and NS-GNP showed the corresponding value 40.87 µg/ml and 64 µg/ml, equivalent to ascorbic acid, standard calibration graph is shown in

(Fig.7).

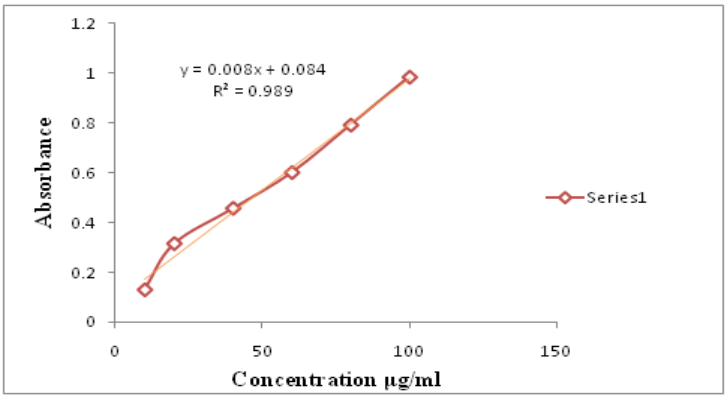

Figure 7: Standard calibration graph of Ascorbic acid for the estimation of FRAP assay

The DPPH inhibition percentage represents the antioxidant activity of N. stellata plant extract and gold nanoparticles. Comparing the plant extract to the gold nanoparticles revealed powerful free radical scavenger. The IC50 value was found to be 75.75±1.48 for NS-GNP and 90.4±1.21 for NS extract. Ascorbic acid was standard, and percentage inhibition graph of NS plant extract & synthesized NS-GNP is shown in (Fig. 8).

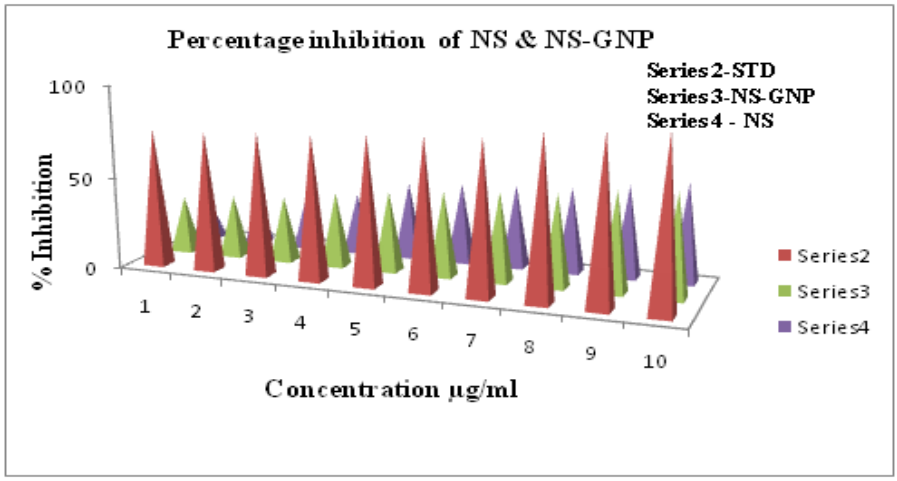

Figure 8: Percentage inhibition graph of NS plant extract & synthesized NS-GNP

4.4. In vitro analysis of NS-GNP against HepG2 cell lines: Based on the results obtained from the MTT assay, it was observed that when the HepG2 cell line was exposed to different concentrations of the sample. The study aimed to assess the inhibitory potential of gold nanoparticles derived from N. stellata extract on the HepG2 cell line. The findings revealed that the synthesized GNP demonstrated an IC50 value of 95.74 ± 0.03µg/ml, indicating their capacity to effectively inhibit the growth of HepG2 cells at this concentration (Fig. 9). These results underscore the in-vitro cytotoxicity of NS-GNP against the HepG2 liver cancer cell line. The concentration-dependent effect of the GNP on HepG2 cells was evident, suggesting that lower concentrations result in reduced cell growth inhibition, while higher concentrations may yield a

more pronounced effect. With an IC50 value below 100 µg/ml, the study indicates the substantial in-vitro cytotoxic potential of the N.stellata extract loaded GNP against HepG2 cells, thus warranting further investigation (Paul et al., 2018). Photos were captured by (Olympus ek2, using Camera, Am Scope digital camera 10 MP Aptima CMOS).

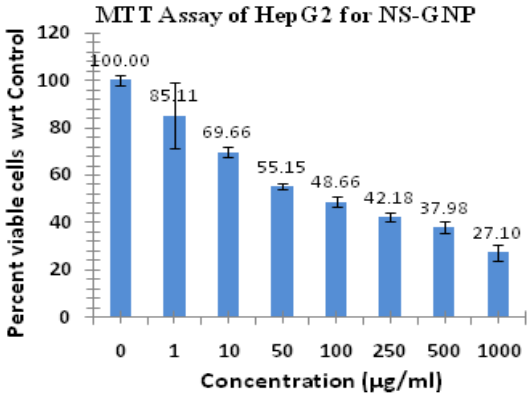

Figure 9: Representation of % cell viability Vs concentration plot of NS-GNP

5. Conclusion:

Overall, this research sets the stage for utilizing N. stellata as a resource for producing biocompatible gold nano particles with potential applications in liver cancer therapy. With further exploration and optimization, this approach could contribute to the development of novel and effective cancer treatment strategies.

Acknowledgements: Authors would like to acknowledge the Sam Higginbottom University of Agriculture, Technology &Sciences, Prayagraj, India, for providing facilities to complete this study.

Conflicts of interest/Competing interests: The authors declare no competing interest

Code availability: NA

Authors' contributions: Conceptualization: Amita Verma, Rohit Tripathi; Data collection: Rohit Tripathi, Sudheer Kumar, Bhupendra Singh; Writing the manuscript: Rohit Tripathi, Arpita Yadav, Vikas Kumar; Sketching of figures and data interpretation: Rohit Tripathi, Arpita Yadav; Review and final editing of the manuscript: Amita Verma.

Funding information: NA

Abbreviations:

NS	*Nymphaea stellata, N.stellata*
DLS	Dynamic light scattering
FT-IR	Fourier-transform infrared spectroscopy
HepG2	Human liver cancer cell lines

NS-GNP	*Nymphaea stellata*-Gold nano particles
SEM	Scanning electron microscopy
TEM	Transmission Electron Microscope

References

1. Antonisamy, P., Subash-Babu, P., Alshatwi, A. A., Aravinthan, A., Ignacimuthu, S., Choi, K. C., & Kim, J. H. (2014). Gastroprotective effect of nymphayol isolated from Nymphaea stellata (Willd.) flowers: contribution of antioxidant, anti-inflammatory and anti-apoptotic activities. Chemico-Biological Interactions, 224, 157-163.
2. Baby, J., Devan, A. R., Kumar, A. R., Gorantla, J. N., Nair, B., Aishwarya, T. S., & Nath, L. R. (2021). Cogent role of flavonoids as key orchestrators of chemoprevention of hepatocellular carcinoma: A review. Journal of Food Biochemistry, 45(7), e13761.
3. Babbar, N., Oberoi, H. S., Uppal, D. S., & Patil, R. T. (2011). Total phenolic content and antioxidant capacity of extracts obtained from six important fruit residues. Food research international, 44(1), 391-396.
4. Bhattacharjee, S. (2016). DLS and zeta potential–what they are and what they are not?. Journal of controlled release, 235, 337-351.
5. Biharee, A., Bhartiya, S., Yadav, A., Thareja, S., & Jain, A. K. (2023). Microsponges as Drug Delivery System: Past, Present, and Future Perspectives. Current pharmaceutical design, 29(13), 1026-1045.
6. Czeczot, H., Tudek, B., Kusztelak, J., Szymczyk, T., Dobrowolska, B., Glinkowska, G., & Strzelecka, H. (1990). Isolation and studies of the mutagenic activity in the Ames test of flavonoids naturally occurring in medical herbs. Mutation Research/Genetic Toxicology, 240(3), 209-216.
7. Ghany, M. G., Kleiner, D. E., Alter, H., Doo, E., Khokar, F., Promrat, K., & Hoofnagle, J. H. (2003). Progression of fibrosis in chronic hepatitis C. Gastroenterology, 124(1), 97-104.
8. Goldstein, A., Soroka, Y., Frušić-Zlotkin, M., Popov, I., & Kohen, R. (2014). High resolution SEM imaging of gold nanoparticles in cells and tissues. Journal of microscopy, 256(3), 237-247.
9. Grela, E., Kozłowska, J., & Grabowiecka, A. (2018). Current methodology of MTT assay in bacteria–A review. Acta histochemica, 120(4), 303-311.
10. Guo, C., Yang, J., Wei, J., Li, Y., Xu, J., & Jiang, Y. (2003). Antioxidant activities of peel, pulp and seed fractions of common fruits as determined by FRAP assay. Nutrition research, 23(12), 1719-1726.
11. Grela, E., Kozłowska, J., & Grabowiecka, A. (2018). Current methodology of MTT assay in bacteria–A review. Acta histochemica, 120(4), 303-311.
12. Jans, H., Liu, X., Austin, L., Maes, G., & Huo, Q. (2009). Dynamic light scattering as a powerful tool for gold nanoparticle bioconjugation and biomolecular binding studies. Analytical chemistry, 81(22), 9425-9432.
13. Kalita, P., Tapan, B. K., Pal, T. K., & Kalita, R. (2013). Estimation of total flavonoids content (TFC) and anti oxidant activities of methanolic whole plant extract of Biophytum sensitivum Linn. Journal of Drug delivery and Therapeutics, 3(4), 33-37.
14. Kubiak, K., Adamczyk, Z., Maciejewska, J., & Oćwieja, M. (2016). Gold nanoparticle monolayers of controlled coverage and structure. The Journal of Physical Chemistry C, 120(22), 11807-11819.
15. Loncaric, A., Celeiro, M., Jozinović, A., Jelinić, J., Kovač, T., Jokić, S., & Lores, M. (2020). Green extraction methods for extraction of polyphenolic compounds from blueberry pomace.

Foods, 9(11), 1521.
16. Losic, B., Craig, A. J., Villacorta-Martin, C., Martins-Filho, S. N., Akers, N., Chen, X., & Villanueva, A. (2020). Intratumoral heterogeneity and clonal evolution in liver cancer. Nature communications, 11(1), 291.
17. Mahakham, W., Theerakulpisut, P., Maensiri, S., Phumying, S., & Sarmah, A. K. (2016). Environmentally benign synthesis of phytochemicals-capped gold nanoparticles as nanopriming agent for promoting maize seed germination. Science of the Total Environment, 573, 1089-1102.
18. Paul, P., Chatterjee, S., Pramanik, A., Karmakar, P., Chandra Bhattacharyya, S., & Kumar, G. S. (2018). Thionine conjugated gold nanoparticles trigger apoptotic activity toward HepG2 cancer cell line. ACS Biomaterials Science & Engineering, 4(2), 635-646.
19. Petibois, C., Cazorla, G., Cassaigne, A., & Déléris, G. (2001). Plasma protein contents determined by Fourier-transform infrared spectrometry. Clinical Chemistry, 47(4), 730-738.
20. Raja, M. M. M., Sethiya, N. K., & Mishra, S. H. (2010). A comprehensive review on Nymphaea stellata: A traditionally used bitter. Journal of advanced pharmaceutical technology & research, 1(3), 311-319.
21. Saravanan, G. O. V. I. N. D. A. R. A. J., Alagarsamy, V. E. E. R. A. C. H. A. M. Y., & Prakash, C. R. (2010). Synthesis and evaluation of antioxidant activities of novel quinazoline derivatives. Int J Pharm Pharm Sci, 2(4), 83-86.
22. Schmidt, W. (2009). Calculation of XRD patterns of simulated FDU-15, CMK-5, and CMK-3 carbon structures. Microporous and mesoporous materials, 117(1-2), 372-379.
23. Singh, K., Biharee, A., Vyas, A., Thareja, S., & Jain, A. K. (2022). Recent advancement of polymersomes as drug delivery carrier. Current pharmaceutical design, 28(20), 1621-1631.
24. Thorgeirsson, S. S., & Grisham, J. W. (2002). Molecular pathogenesis of human hepatocellular carcinoma. Nature genetics, 31(4), 339-346.
25. Zimbone, M., Calcagno, L., Messina, G., Baeri, P., & Compagnini, G. (2011). Dynamic light scattering and UV–vis spectroscopy of gold nanoparticles solution. Materials Letters, 65(19-20), 2906-2909.